THE JOURNAL OF PHYSICAL CHEMISTRY B

Article

pubs.acs.org/JPCB

Colloidal Aggregate and Gel Incubated by Amorphous Conjugated Polymer in Hybrid-Solvent Medium

Rong H. Guo,[†] Chih H. Hsu,[†] Chi C. Hua,*[,†] and Show A. Chen[‡]

[†]Department of Chemical Engineering, National Chung Cheng University, Chiayi 621, Taiwan, Republic of China

[‡]Department of Chemical Engineering, National Tsing Hua University, Hsinchu 300, Taiwan, Republic of China

Supporting Information

ABSTRACT: A practical valuable amorphous conjugated polymer, poly(2-methoxy-5-(2′-ethylhexyloxy)-1,4-phenylenevinylene (MEH-PPV), has been revealed to foster an abundance of micrometer-sized colloidal aggregates at relatively low concentration (below 1 wt %) in a hybrid-solvent medium that contains a nonsolvent, and the solution turned into gel by colloidal bridging after one-day aging at 30 °C. In contrast with typical polymer gels fostered by (anisotropic) chain cross-linking or planar packing on selective interacting sites, the MEH-PPV gel has been revealed (via dynamic light scattering, small-angle light scattering, time-sweep dynamic modulus and optical microscope) to first develop featureless aggregate clusters in solution and, as the solvent quality worsens with reduced system temperature, bridge themselves to form gel through a one-dimensional (1-D) to three-dimensional (3-D) kinetic pathway. Combined dynamic/static light scattering analyses, along with supporting scanning electron microscope image and molecular dynamics simulation, indicated a concomitant structural reorganization *within* the colloidal aggregates, where spontaneous chain packing was perceived to form local fiber-like materials that are elastic by nature (i.e., a *q*-independent decay rate). The near coincidence of the above-mentioned microscopic and macroscopic phase alterations led us to contend that similar fibrous materials have served as the exterior bridging agent to fabricate colloidal strands upon gelation. The present findings clarify previously enigmatic, much speculative, gelation phenomena of MEH-PPV, and shed light on the prospect of capitalizing on specific polymer−solvent interactions to incubate desirable colloidal aggregates and gels in room-temperature processing of practical valuable conjugated polymers.

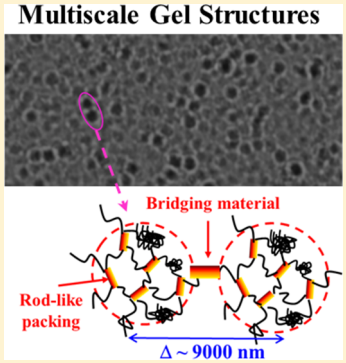

1. INTRODUCTION

Conducting conjugated polymers have currently served as the main active materials in fabricating solution-processed polymer light-emitting diodes (PLED)[1−3] and plastic solar cells.[4−6] The intrinsic chain stiffness and amphiphilic nature of commonly used conjugated polymers, however, have substantially diversified their solution properties, permitting a wide variety of (intra- and interchain) aggregate species and phase morphologies. Given that the photophysics of solution-cast thin films can be drastically influenced by their microstructures in solution state,[7,8] efforts toward understanding the detailed solution properties have since invoked various analyzing schemes including spectroscopy,[9−11] small-angle neutron/X-ray scattering,[12−15] light scattering,[16−18] and computer simulation.[19−21] At the same time, conjugated polymer gels have attracted growing interest because of their ability to summon an unusual combination of physical properties, such as rubber-like elasticity, swelling/deswelling in volume, and, in particular, specific transport properties ascribed to the presence of a three-dimensional (3-D) network.[22−24] Recently, a number of studies have reported novel optoelectronic devices making use of polymer gels as the active layer.[25−29] In a future perspective, gel processing of conjugated polymers under proper solvent mediation, balanced mechanical stress, and system temperature can be anticipated to help substantially promote the uniformity of chain alignment and the often desirable percolation network crucial for future advancement in organic photophysics.[30,31]

Recent studies on conjugated polymer gels have been focused on the crystalline types of polymers, such as polythiophenes,[32−37] poly(phenylene-ethynylene)s,[38,39] and polyfluorenes.[40,41] Gels produced from an amorphous conjugated polymer like poly(2-methoxy-5-(2′-ethylhexyloxy)-1,4-phenylenevinylene (MEH-PPV), in contrast, were occasionally reported under somewhat "harsh" experimental conditions (e.g., under prolonged low-temperature storage[42] or following the cessation of long-term flow shearing[43]) and have received no systematic exploration to date. Lacking prominent anisotropic interactions (such as hydrogen bonding and $\pi-\pi$ interaction) in solution state,[20] MEH-PPV and the like, conceivably, are not good gelators. Recently, MEH-PPV solution was reported to turn into gel after one-day aging in a hybrid-solvent medium that consists of a nonsolvent (alkanes).[44,45] Although adding poor- or nonsolvents may help promote interchain aggregation and thus lift the possibility of creating a gel phase, too poor a solvent quality would presumably lead to dominant *intrachain* aggregates unfavorable

Received: January 20, 2015
Published: January 21, 2015

DOI: 10.1021/acs.jpcb.5b00575
J. Phys. Chem. B 2015, 119, 3320−3331

for gelation. In general, therefore, one might expect a sophisticated interplay of two mixing solvents in incubating MEH-PPV gels. From a technological perspective, this gelation phenomenon is of particular interest because it requires only a room-temperature aging process of relatively dilute sample solutions (i.e., below 1 wt %).

Prior research on organogels has often found it necessary to utilize multiscale experimental protocols.[32,46−49] Among them, dynamic/static light scattering (DLS/SLS)[50−52] and rheological characterizations[32,53] represent two readily accessible and mutually complementary schemes, and have proven to be especially powerful to simultaneously explore kinetic and structural features during a sol−gel transition. Computer simulations, on the other hand, have recently shown promising prospect of deciphering essential microstates that later trigger a bulk phase transition.[54] Herein, we demonstrate that a combination of DLS/SLS, SALS (small angle light scattering) and time-sweep dynamic modulus measurements enables one to establish a comprehensive picture describing the structural evolutions during MEH-PPV so-gel transition in a hybrid-solvent medium. The analyses have been reinforced by observations from optical microscope (OM) and scanning electron microscope (SEM) imaging and molecular dynamics simulation, with the central findings as follows. Unlike typical polymer gels known to be bolstered by chain cross-linking or $\pi - \pi$ packing on selective interacting sites,[55] the MEH-PPV gel fostered from a hybrid-solvent medium evidently utilized micrometer-sized colloidal aggregates in solution as the seed particles, which, upon quenching to the gelation temperature at 30 °C, further associated themselves in a one-dimensional (1-D) to 3-D pathway to forming gel, as can be clearly viewed by the OM image to embody an interconnected, percolated colloidal network. To our knowledge, only biological polymers were known to utilize a similar pathway of colloidal bridging to form gels, involving yet smaller (nanometer-sized) aggregates and anisotropic binding sites.[56,57] The present findings not only clarify previously enigmatic, much speculative, gelation phenomena of MEH-PPV, but also shed light on the prospect of capitalizing on peculiar solvent media to incubate desirable colloidal aggregates and gels in room-temperature processing of practical valuable conjugated polymers.

2. EXPERIMENTAL METHODS

2.1. Materials and Sample Preparation. The MEH-PPV sample was purchased from Aldrich Chemical and has a reported number-average molecular weight 150 000−250 000 g/mol and polydispersity index about 5. Each of the two solvents used, chlorobenzene and nonane (Aldrich Chemical), was filtered through a 0.22 μm PVDF Millipore filter to remove dust. The sample vials were washed with detergent and then treated with filtered deionized (DI) water. MEH-PPV sample solution with a concentration of 9 mg/mL was prepared with filtered hybrid solvent consisting of chlorobenzene and nonane with a volume ratio of 5:3 (a general discussion about the effects of the mixing ratio can be found elsewhere[44]). The sample solution was sonicated 10 h per day at 60 °C for 4 days and stored in a dark, auto dry box at room temperature. As shown in Figure 1, the MEH-PPV sample solution could be brought to the gel state via aging at 30 °C, and the gel structure may be largely disintegrated by heating back to 60 °C. The freshly prepared, heated solution was allowed to equilibrate for at least 2 h at 60 °C to minimize the effect of prior sonication, and then quickly transferred to the sample carriers for all

Figure 1. Photographs of MEH-PPV solution for (a) a fresh sample at 60 °C, (b) after aging for 1.5 h at 30 °C, and (c) after aging for 25 h at 30 °C.

subsequent characterizations. Most measurements, as described in the following subsections, were conducted during stepwise cooling from 60 to 30 °C, and the sample was allowed to stand still for 30 min prior to each individual measurement. Upon reaching the gelation temperature at 30 °C, the effects of aging time were closely monitored, until the gel network ripened after about one-day aging. The effect of varying thermal history was not investigated, in part because the gel sample is largely thermally reversible, and we expect no major disparity in the conclusions thus drawn.

2.2. Laser Light Scattering (DLS/SLS). Light scattering measurements were performed on a laboratory-built apparatus as described elsewhere.[17] The instrument was equipped with a photon counting photomultiplier tube (Hamamatsu, H7155) linked to a counting board (Hamamatsu, M9300), and a 15 mW polarized He−Ne laser (λ_0 = 632.8 nm) was initially used as the incident light. As detailed in the Supporting Information (SI, Figures S1−S2), the effect of incident light intensity has been scrutinized, ensuring that the data reported were unaffected by absorption and, consequently, thermal-induced flow convection.[58] Moreover, ergodicity of MEH-PPV gel was assessed using the partial heterodyne method[50,51] (Figure S3 in the SI). Accordingly, the laser power was finally attenuated to be about 0.2 mW for all light scattering experiments, and the sample cell with an inner diameter of 8 mm (Hellma, 540.111) was placed in an index-matching vat containing decalin to remove unwanted surface reflection or refraction.

The normalized intensity autocorrelation function, $g^{(2)}(q,t)$, collected in a homodyne DLS experiment can be related to the normalized field autocorrelation function, $|g^{(1)}(q,t)|$, through the Siegert relation: $g^{(2)}(q,t) = 1 + \beta|g^{(1)}(q,t)|^2$,[59,60] where β ($0 < \beta < 1$) is the spatial coherence factor depending on the detection optics, and $q = (4\pi n/\lambda_0)\sin(\theta/2)$ is the scattering vector with n the refractive index of the dispersion medium and λ_0 the wavelength of the incident light in vacuum.

In general, $|g^{(1)}(q,t)|$ may be expressed in terms of the decay time distribution function, $A(\tau)$, as[60]

$$|g^{(1)}(q, t)| = \int_0^\infty A(\tau)\exp(-t/\tau)\,\mathrm{d}\tau \quad (1)$$

where $A(\tau)$ represents the intensity-weighted contribution associated with the decay time constant τ. In the case of multiple relaxation processes, the detailed distribution may be obtained by Laplace inversion, and the individual modes are typically retrieved from the commercial software CONTIN.[61] The average decay time of each individual mode can be evaluated by the relation $\langle\tau_i\rangle = ((\Sigma_n A_n(\tau)\tau_n)/(\Sigma_n A_n(\tau)))$, where the index n sums over the entire regime that has been assinged to the ith mode.

For gel systems commonly embodying multiple relaxation modes, combination of DLS and SLS data can be utilized to

DOI: 10.1021/acs.jpcb.5b00575
J. Phys. Chem. B 2015, 119, 3320−3331

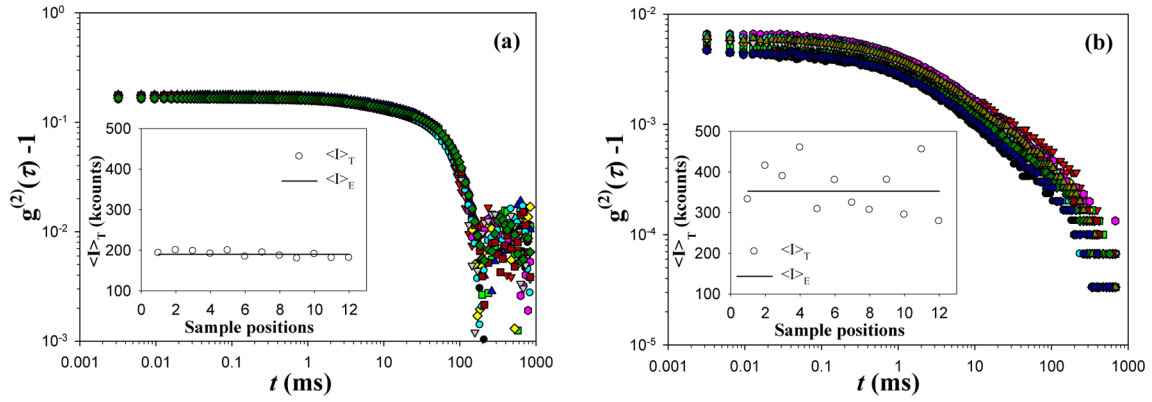

Figure 2. Light scattering intensity correlation functions at $\theta = 30°$ for (a) solution and (b) gel (24-h aging) as measured from different sample positions. The inset figures compare the time ($\langle I \rangle_T$) and ensemble ($\langle I \rangle_E$) averages to show the effect of nonergodicity.

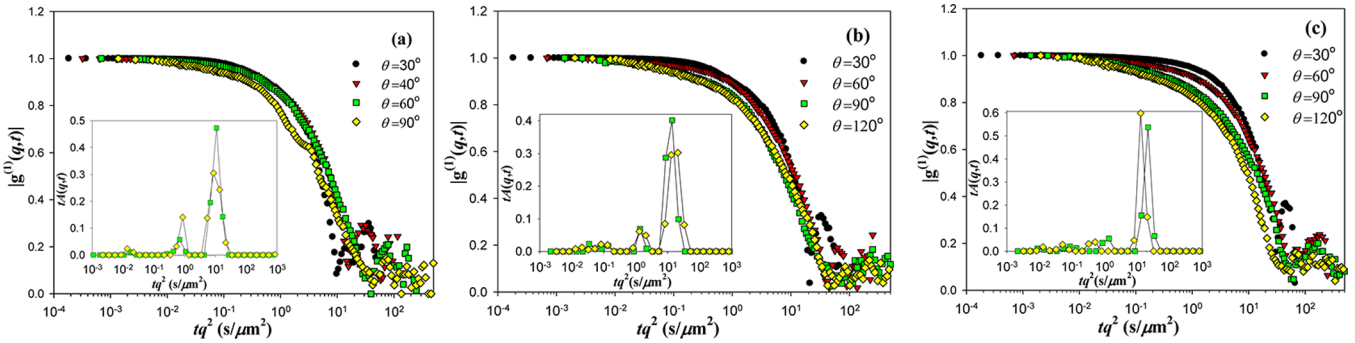

Figure 3. Angular dependences of field autocorrelation function for MEH-PPV solution at (a) 60 °C, (b) 50 °C, and (c) 40 °C, where the decay time t has been rescaled with q^2. To visualize the existence of three major modes, the decay time distributions $A(q,t)$ as extracted from CONTIN for two representative scattering angles are provided in the inset.

simultaneously explore their dynamic and structural features.[62−64] Specifically, the intensity, $I_i(q)$, contributed by the ith relaxation mode can be obtained via

$$I_i(q) = I(q)\frac{\sum_n A_n(\tau)}{\text{sum\_}A} \tag{2}$$

where $I(q)$ is the total scattering intensity from SLS experiment, $A_n(\tau)$ is obtained from DLS experiment at the same scattering angle q and has a significance as above, and the denominator sum_A sums over all modes. Accordingly, the average decay rate $\langle \Gamma_i \rangle$ can be defined as the inverse of $\langle \tau_i \rangle$: $\langle \Gamma_i \rangle = 1/\langle \tau_i \rangle$, and its q dependence may be expressed by $\langle \Gamma_i \rangle \sim q^{\alpha}$. While the q dependence of Γ_i reveals the specific relaxation mechanism, e.g., $\alpha = 2$ for diffusive motions, $I_i(q)$ provides knowledge of the corresponding structural feature such as the fractal dimension.

2.3. Small Angle Light Scattering (SALS). SALS measurements may complement the usual SLS experiment in exploring large aggregate clusters (in solution) and other structural features (in gel state) that bear characteristic length scales falling in the micrometer range. The setup of the SALS apparatus used in this study resembles the one reported in prior work.[65] A 2 mW He−Ne laser with a wavelength of $\lambda_0 = 632.8$ nm and a beam diameter of 0.8 mm was used as the incident light, which was guided through a spatial filter to enhance beam homogeneity. Detailed descriptions about the setup, calibration, and analyzing scheme of this apparatus can be found in the SI (Figures S4−S6).

2.4. Dynamic Modulus Measurement. Oscillatory shear measurements were performed on a DHR-2 rheometer (TA Instruments). An aluminum double-gap cylinder geometry was used to acquire data as the viscosity of MEH-PPV solution was typically low. The inner cup of the geometry has a diameter of 30.2 mm, and the inner and outer rotor diameters are 31.97 and 34.98 mm, respectively. The sample was loaded via pipet into the cup, and both gaps bear the same size of 0.95 mm after immersing the cylindrical rotor with a height of 53 mm. The above geometry was equipped with a Peltier temperature controller, and was preheated to 60 °C prior to loading the fresh sample. To minimize the effect of solvent evaporation, solvent trap was utilized during the entire measuring process. Viscoelastic properties of MEH-PPV solution and gel were measured using three different rheological modes: strain sweep with an angular frequency of 1 rad/s was used to identify the linear viscoelastic regime as the sample solution had been converted to the gel state at 30 °C. Oscillation frequency sweep was subsequently conducted with a (linear) strain amplitude of 0.3 to explore the variations of G' (storage modulus) and G'' (loss modulus) from solution to the gel state. Finally, the aging-time dependent, time-sweep complex modulus data of MEH-PPV gel at 30 °C were closely monitored using a strain amplitude of 0.3 at two different frequencies, 1 and 10 rad/s. Note that the general trends of the viscometric features have been verified by using a parallel-plate fixture (with plate diameter of 20 mm and gap distance of 1 mm) for the gel sample.

DOI: 10.1021/acs.jpcb.5b00575
J. Phys. Chem. B 2015, 119, 3320−3331

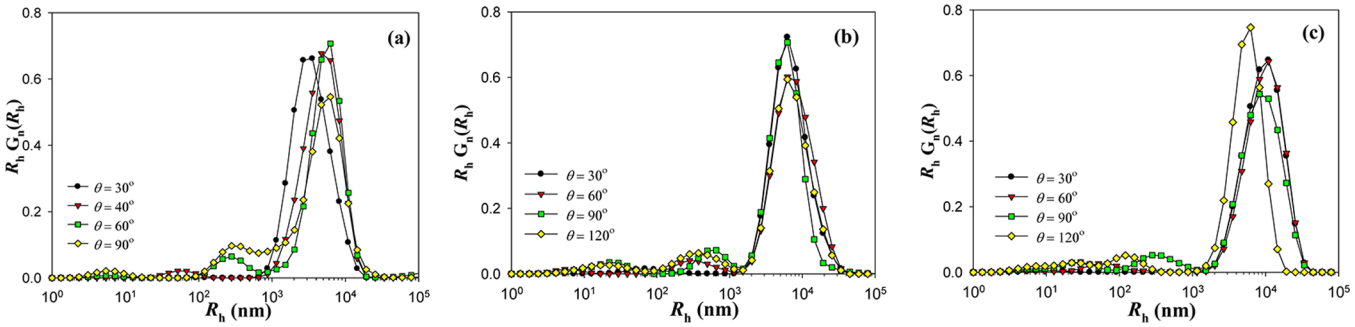

Figure 4. Intensity-weighted distributions of the hydrodynamic radius for (a) 60 °C, (b) 50 °C and (c) 40 °C, where the ordinate has been multiplied by R_h in order to make the "visual" areas in each figure better reflect the actual ones on a logarithmic scale.

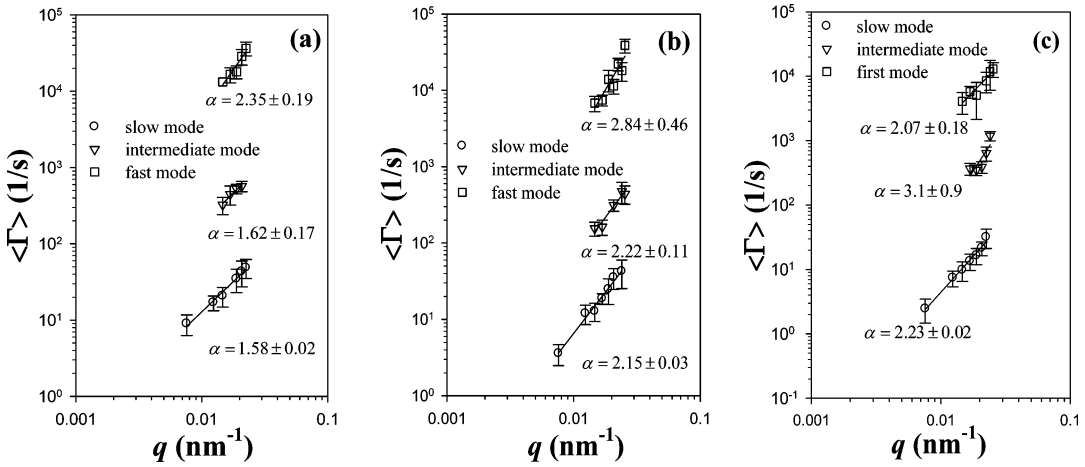

Figure 5. Decay rate ($\langle\Gamma\rangle = \langle\tau\rangle^{-1}$) as a function of the scattering vector q for the MEH-PPV solution at (a) 60 °C, (b) 50 °C, and (c) 40 °C.

3. RESULTS AND DISCUSSION

3.1. Identification of Sol−Gel Transition. In addition to the flow experiment shown in Figure 1 and the viscometric features discussed in a later subsection that can be utilized to identify a sol−gel transition of MEH-PPV solution, several characteristic DLS features as had been reported in the literature[51,66−70] can be clearly seen with the results shown in Figure 2. These include a generally promoted scattering intensity, position-dependent scattering intensity fluctuations (i.e., nonergodicity) and a reduced initial value of $g^{(2)}(q,t) - 1$ (and thus β for $|g^{(1)}(q,t)|$), as the system has been brought from solution to the gel state. In interesting contrast, however, an often observed transition from stretched-exponential to power-law dependence of $g^{(2)}(q,t) - 1$ is clearly absent, and the expected power-law behavior remains unobservable even after prolonged aging of the MEH-PPV gel. The last feature appears to suggest there was no divergence of the relaxation time associated with the slow (gel) mode upon gelation.[66] Reasons to this disparity become more transparent as the position-independent scattering function $|g^{(1)}(q,t)|$ (see also Figure S3b in the SI) from solution to the gelling state is further analyzed below.

3.2. Diffusive Aggregates in Solution. We first examined the field autocorrelation functions, $|g^{(1)}(q,t)|$, of MEH-PPV solution during stepwise cooling from 60 to 40 °C to unveil the aggregate properties as well as their structural development toward the gel state at 30 °C. As shown in Figure 3, $|g^{(1)}(q,t)|$ at various scattering angles do not collapse into a single curve after the decay time has been rescaled with q^2, suggesting that the contribution from internal segmental motions and/or the effect of polydispersity in aggregate size must be at play, as also reflected in a later analysis of the CONTIN modes. To simultaneously cope with these effects, a prior study had introduced a self-consistent formulation for analyzing the dynamic structure factor in DLS experiments on two standard MEH-PPV solutions (with toluene or chloroform as the solvent).[17]

Within this formulation, it can be seen from Figure 4 that the mean hydrodynamic radius of the aggregate species increases notably with reduced system temperature. Note, in particular, that the mean aggregate sizes all fall in the micrometer range (which has been confirmed by the OM image shown in Figure S10 of the SI as well as by the SALS analysis discussed later). For comparison, the DLS results for 9 mg/mL MEH-PPV/chlorobenzene solution (i.e., without the nonsolvent nonane) are provided in the SI (Figures S7−S8). The general observation has been that the mean aggregate size is much smaller and less dependent on the system temperature. In particular, there were no apparent changes with aging time at 30 °C, the gelation temperature for the hybrid-solvent system.

For the results shown in Figure 3, three major modes retrieved from CONTIN deserve further inspection. These modes have also been suggested by independent analysis based on nonlinear regression method as described in prior work.[17] Figure 5 shows the q-dependence of the average decay rate, $\langle\Gamma_i\rangle \sim q^{\alpha}$, for each mode. By taking into account the effect of polydispersity, as reflected in the error bar of individual datum point, these modes are clearly diffusive by nature as the scaling exponents all fall around −2. Thus, the significance of these modes was confirmed (CONTIN analysis sometimes yields

DOI: 10.1021/acs.jpcb.5b00575
J. Phys. Chem. B 2015, 119, 3320−3331

artificial modes without practical physical meaning). The results yielded aggregate species of three distinct sizes: R_h = 20−50 nm, R_h = 200−300 nm, and R_h = 2000−6000 nm. By keeping track of these modes during the so-gel transition, one can, in principle, illuminate the pathway and structural evolution of MEH-PPV gelation. Of particular interest is the micrometer-sized aggregate that dominates the DLS signal and can thus be unmistakably identified in all cases.

Another aspect of MEH-PPV solution that is relevant for deciphering the factors driving a sol−gel transition is concerned with the structural compactness of the aggregate clusters. Figure 6 shows that the reduced first cumulant, as extracted

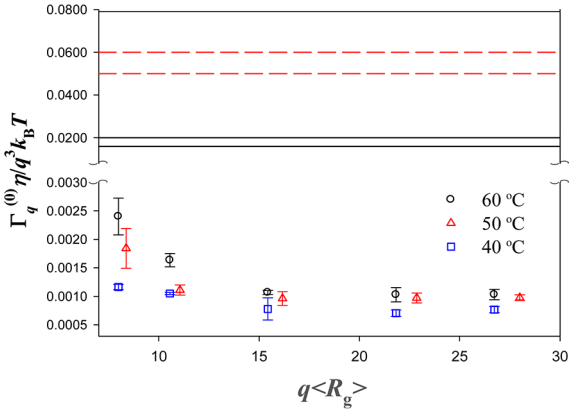

Figure 6. Reduced first cumulant $\Gamma_q^{(0)}\eta/q^3k_BT$ as a function of the scattering angle for hybrid-solvent MEH-PPV solution (η being the temperature-dependent solvent viscosity). For comparison, the solid lines and dashed lines mark the ranges of previously determined values at $q\langle R_g\rangle \gg 1$ for 3 mg/mL MEH-PPV/toluene[17] and 3 mg/mL polystyrene/toluene,[71] respectively.

from the initial decay rate $\Gamma_q^{(0)} = (\partial/(\partial t))\ \ln|g^{(1)}(q,t)||_{t=0}$, eventually levels off (i.e., exhibiting a q^3 dependence) at large values of $q\langle R_g\rangle$ ($\langle R_g\rangle$ being the number-average radius of gyration as extracted from a later SALS analysis). In particular, its height drops appreciably with reduced system temperature, suggestive of increasingly suppressed internal motions and, hence, a more compact interior structure. In fact, the reduced first cumulants for the hybrid-solvent MEH-PPV solution are substantially smaller than those for MEH-PPV/chlorobenzene solution (see Figure S9 in the SI) and most known polymer solutions. For instance, as can be seen in Figure 6, the values are an order of magnitude lower than what had previously been found for dilute MEH-PPV/toluene solution, which, in turn, bears an average value three times lower than the counterpart polystyrene solution.

To summarize, we note that the hybrid-solvent medium under investigation appears to achieve two important functions essential for the gelation of MEH-PPV. First, it helps foster and sustain, with ideally compromised solvent qualities (see Figure S13 and related discussion in SI), micrometer-sized colloidal aggregates previously unobserved with other MEH-PPV solution systems. Second, the somewhat extreme structural compactness realized near the gelation temperature (which is about 20 times more compact than that of a comparative MEH-PPV/toluene solution) eventually triggered a microscopic as well as macroscopic phase transition, as we elucidate in the following subsections. This situation may be compared with the microphase alternation recently predicted for entangled MEH-PPV solutions[54] (see also Figure S14 in SI), as the system free energy starts to be dominated by interchain packing.

3.3. Structural Evolutions in Gel State. *3.3.1. DLS Features.* Figure 7a,b shows the field autocorrelation functions $|g^{(1)}(q,t)|$ for two different aging times at the gelation temperature; the decay time distributions $A(q,t)$ extracted from CONTIN for two representative scattering angles are also shown. Given that three diffusive modes have previously been identified for the solution sample, it seems rational to keep track of these individual modes in the gel sample. From the results shown in Figure 7a,b, it seems that the existence and distinction of three major modes become even evident for the gel sample. This evolving feature in the CONTIN modes can be rationalized by noting that, in pure diffusive dynamics, large aggregate clusters dominated the contribution to the DLS signal, whereas their influence waned as a result of arrested particle motions, as indicated by the following analysis.

Figure 7c,d compares the CONTIN modes for the solution and gel samples. We have adopted the same denomination as given in Figure 5 for each mode according to the results of properly renormalized average decay rate. It should be borne in mind, however, that due to the difficulty of precisely matching the CONTIN modes of two distinct physical states (i.e., solution vs gel), only the ubiquitously dominant slow mode may be unambiguously associated with micrometer-sized colloidal aggregates. Except for the fast mode, which changes less significantly throughout the entire gelation process, the other two modes clearly become nondiffusive in nature, as the scaling exponents now deviated little from zero within experimental uncertainties. At first sight, one might regard the altering scaling behavior as signature of those relatively large aggregate clusters being arrested upon gelation. Indeed, a later SALS analysis and the OM image both confirmed the mutual binding between different micrometer-sized colloidal aggregates. The following analysis of combined DLS/SLS data, however, points to the possibility that the arrested *intermediate* mode denotes newly developed fibrous materials within previously featureless aggregate clusters. Considering that the fast mode is the most susceptible to the interferences from the other two modes and, in particular, plays insignificant role in the formation of gel, we shall focus our attention on the intermediate and the slow modes in the ensuing discussion.

Before closing the discussion with Figure 7, we note that the peculiar relaxation dynamics $\langle\Gamma\rangle = q^0$ had been reported for various polymer solution systems under widely varying physical conditions. First, the reptation motion in a concentrated, entangled system is known to be characterized by a q-independent relaxation dynamics.[72] Similar *viscoelastic* responses of the slow mode in DLS experiments were observed for many polymer associating systems.[73−77] Among them, a q-independent slow-mode relaxation had been ascribed to chain conformational relaxation[76] or stronger segmental interaction near the entanglement nodes.[77] In common, these phenomena seemed to involve either elastic responses due to the formation of physical bonds, or chain relaxations subject to physical confinements. Bearing these features in mind, we next explore the underlying structural features of MEH-PPV gel from a combined DLS/SLS analysis on the intermediate and the slow modes—both exhibited a similar q-independence in their dynamic attributes.

3.3.2. SLS Features. Figure 8a shows the evolution of SLS profiles. Upon gelation, the SLS curve has clearly evolved to embody two distinct power-law regimes. Further shown in

DOI: 10.1021/acs.jpcb.5b00575
J. Phys. Chem. B 2015, 119, 3320−3331

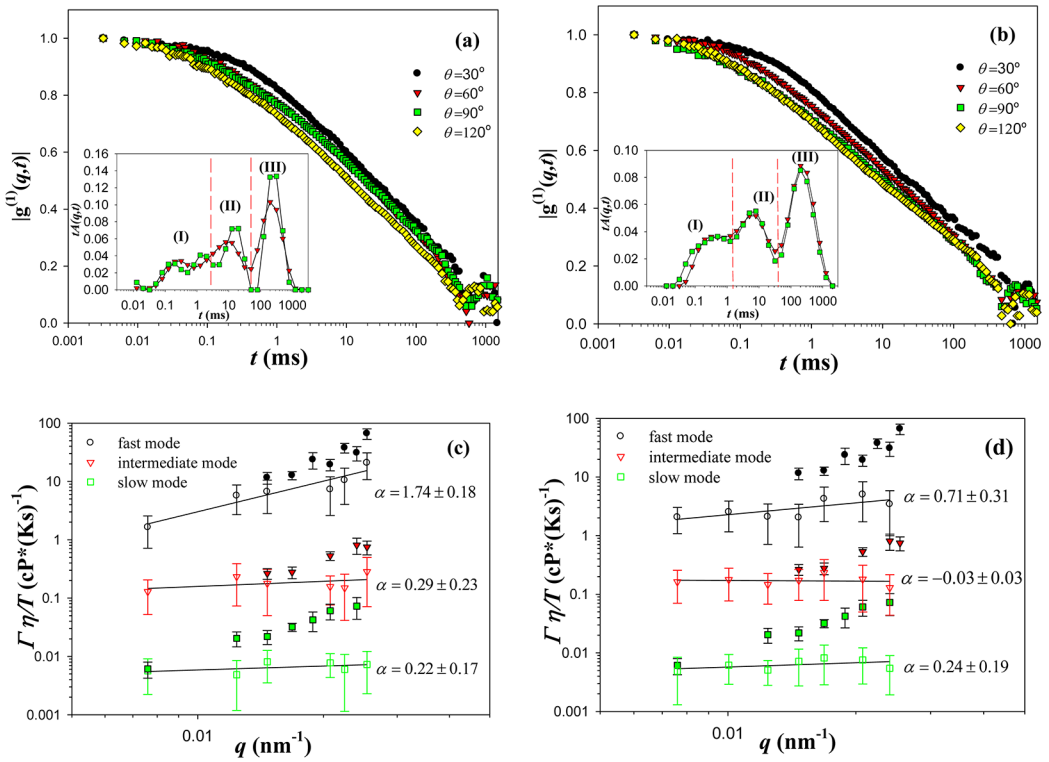

Figure 7. Field autocorrelation function and decay time distribution $A(q,t)$ (shown in the inset for two representative scattering angles) as a function of decay time (t) at 30 °C for two different lengths of aging time: (a) 5 h and (b) 20 h. Three regions marked with (I), (II) and (III) represent the fast, intermediate, and slow modes, respectively. The decay rates ($\langle\Gamma\rangle = \langle\tau\rangle^{-1}$) corresponding to the field autocorrelation functions for (a) and (b) are shown in (c) and (d), respectively. For comparison, the solid symbols represent the decay rates for MEH-PPV solution at 50 °C. Note that the decay rate has been rescaled with the system temperature (T) and solvent viscosity (η).

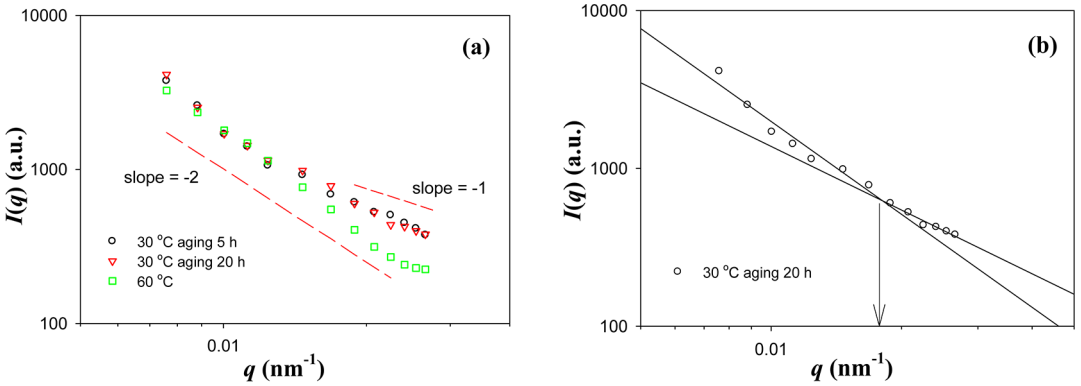

Figure 8. (a) SLS intensity profiles as a function of q from solution to the gel state; (b) the intensity profile as a function of q after 20-h aging at 30 °C.

Figure 8b, the two power-law regimes intersect at a point leading to a characteristic length of $2\pi/q \sim 350$ nm, below which the fractal dimension is suggestive of 1-D structural feature with a scaling exponent of −1.

From the perspective of individual DLS modes, the total scattering intensity $I(q)$ may be so decomposed as to reveal the contributions from the interested intermediate ($I_2(q)$) and slow ($I_3(q)$) modes, respectively, according to eq 2. As shown in Figure 9a, the q dependences of $I_2(q)$ and $I_3(q)$ can be well described by a power law, $I(q) \sim q^{-D_f}$. First, a scaling exponent close to −2 has been found for the slow mode. This mode has previously been identified to be representing micrometer-sized colloidal aggregates, and thus the fractal dimension likely corresponds to the Gaussian interior structure for these aggregates. In contrast, a scaling exponent very close to −1 for the intermediate mode appears to be indicative of local rod-like or fibrous materials constituting the interior network noted above. This essential finding seems to preclude the possibility of linking the diffusive aggregate species as found in Figure 5 with the intermediate mode as explored here for the gel. In summary, the SLS feature seen in Figure 8a along with the above analysis based on combined DLS/SLS data suggest that, upon gelation, the average colloidal aggregate has morphed from a featureless one (i.e., one that constituted by randomized entangled chains) to that embodying local fiber-like structure, which seems elastic by nature for its q-independence in the characteristic decay rate. Further evidence supporting this assertion is discussed below.

DOI: 10.1021/acs.jpcb.5b00575
J. Phys. Chem. B 2015, 119, 3320−3331

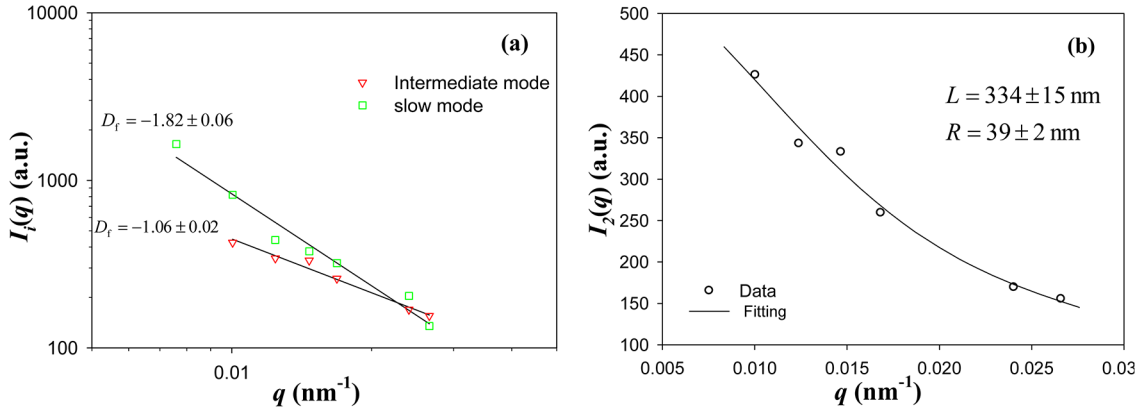

Figure 9. (a) Light-scattering intensities associated with the intermediate (triangle down) and the slow (square) modes, respectively, for the gel sample after 5-h aging. The apparent slope in this plot yields the negative of the fractal dimension, as indicated in the figure; (b) the symbols represent the light-scattering intensities associated with the intermediate mode, and the solid line denotes the fitting with eq 3, yielding parameter values of R and L as indicated in the figure.

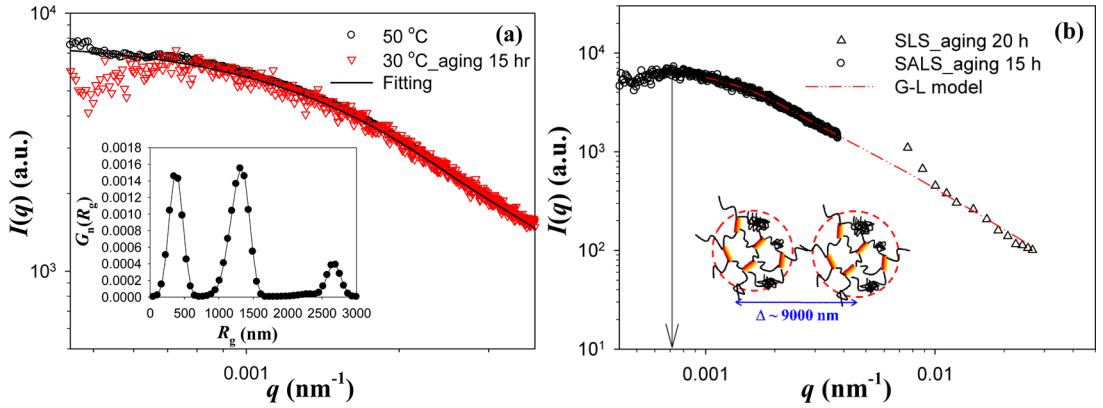

Figure 10. SALS intensity profile as functions of q for (a) the solution sample at 50 °C and the gelling sample at 30 °C, where the inset figure shows the number-weighted size distribution (which yields $\langle R_g \rangle$ = 1101 nm) for the solution sample as extracted from the fitting with eq S2 in the SI; (b) the fitting from eq 5 for combined SALS/SLS data on the gelling sample yields R_g = 1107 ± 8 nm, ξ = 556 ± 4 nm, D = 1.45 ± 0.01, while the arrow denotes the position of q (i.e.,q_{max}) where a maximum SALS intensity occurs.

To quantify the supramolecular fibers hinted at above, the cylindrical form factor was used to fit $I_2(q)$ as $I_2(q) \sim n\Delta\rho^2 V_p^2 P_{cyl}(q)$, where n is the number density of rods, $\Delta\rho$ is the refractive index contrast, and V_p is the volume of each rod. $P_{cyl}(q)$ represents the form factor of randomly oriented cylinders (with radius R and length L) and is given by

$$P_{cyl} = \int_0^{\pi/2} \left[\frac{\sin(qL/2 \cos\varphi)}{qL/2 \cos\varphi} \frac{2J_1(qR \sin\varphi)}{qR \sin\varphi} \right] \sin\varphi \, d\varphi \quad (3)$$

where $J_1(x)$ is the Bessel function of the first kind. For convenience, n, V_p, and $\Delta\rho$ were treated as adjustable parameters, which have no effect on the q dependence of the form factor, as the main purpose of the fitting was to determine the two geometrical parameters R and L. The fitting is displayed by solid line superimposed on the experimental data (points) in Figure 9b. The model is seen to reasonably describe the scattering intensity associated with the intermediate mode. The fitted length for the rods ($L \sim 330$ nm) is in good agreement with a previous estimate based on the crossover of the two power-law regimes in Figure 8b. We note, in passing, the scanning electron microscope (SEM) images of drop-casting film of MEH-PPV gel revealed the prevalence of vein-like morphological feature supportive of the inferred fibrous structure (see Figure S11 in the SI).

For crystalline conjugated polymers, such as P3HT,[32,37] and low-molecular-mass organic gelators,[48,49] fiber-like materials had often been noted to constitute interconnected, percolated gel network. In contrast, MEH-PPV chains have little or no tendency to form fibers under usual experimental conditions. To theoretically assess this possibility for MEH-PPV in a solvent medium identical to the presently investigated one, we have performed atomistic molecular dynamics simulation for a multichain system, as detailed in the SI (see also Figures S12–S13). It is remarkable to observe that, through a sophisticated interplay of two distinct solvent species, random MEH-PPV strands were observed to spontaneously turn into ordered chain packing upon an abrupt quenching to the gelation temperature. The predicted chain reorganization in an originally featureless aggregate appears to echo the changing SLS feature observed in Figure 8a and analyzed in greater detail above. For a considerably enlarged system, Figure S14 in the SI shows a phase-separated, porous microstructure locally bolstered by coarse fibers.

3.3.3. SALS Analysis. The SALS results shown in Figure 10a first confirmed the abundance of micrometer-sized colloidal aggregates in solution. As the sample solution was brought to

DOI: 10.1021/acs.jpcb.5b00575
J. Phys. Chem. B 2015, 119, 3320–3331

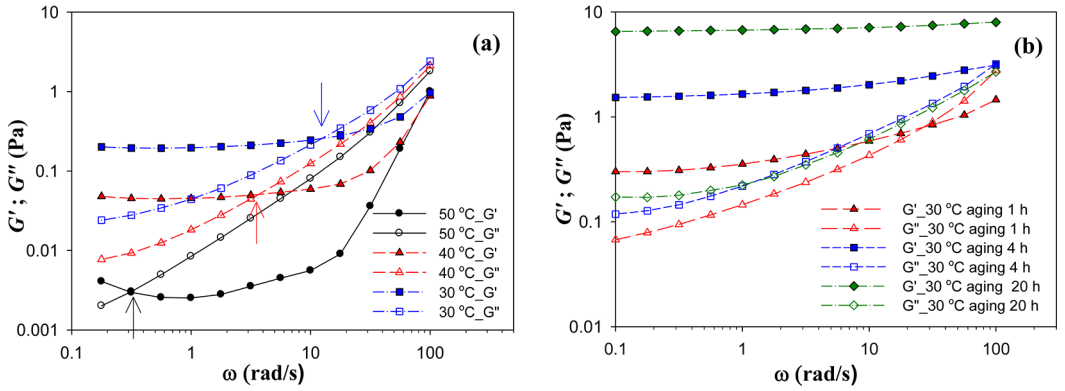

Figure 11. Storage (G') and loss (G'') modulus as functions of angular frequency for (a) solution state, and (b) various gelation stages at 30 °C. The arrows in (a) indicate the crossover of G' and G''.

gelation at 30 °C, the same figure shows the appearance of a distinguishing maximum previously unobserved with the solution sample. The location of this maximum seems independent of the aging time, and thus may be interpreted as an effect of "structure factor" correlating objects that were *spatially* uncorrelated in solution. Often, this structure factor reflects quasi-periodic concentration fluctuations underscored by a characteristic length scale, Λ:[78,79]

$$\Lambda = \frac{2\pi}{q_{\max}} \tag{4}$$

Accordingly, we obtained Λ ∼ 9000 nm as an approximate mean distance between two binding colloidal aggregates (cf. the OM image in Figure S10b in the SI), and thus confirmed a prior DLS interpretation concerning the significance of the arrested slow mode.

Shibayama and co-workers have proposed an extension of Gauss and Lorentz-type functions that bears a general form:[80]

$$I(q) = I_G(0)\exp\left(-\frac{1}{3}R_g^2q^2\right) + \frac{I_L(0)}{\{1 + [(D+1)/3]\xi^2q^2\}^{D/2}} \tag{5}$$

with D reflecting the fractal dimension of the network strands. For comparison, Figure 10b shows that this formula describes reasonably well the combined SALS/SLS data on the gel sample. The parameter values of Rg and ξ are also in good agreement with $\langle R_g\rangle$, and L as have been determined from the fitting in Figure 10a assuming spherical form factor (at low q) and in Figure 9b assuming cylindrical form factor (at high q), respectively. The deviation in the intermediate q range is believed to reflect the Gaussian network structure of the aggregate interior, as discussed previously.

It is of interest to note that, for MEH-PPV solution, SALS analysis suggested little change in $\langle R_g\rangle$ while $\langle R_h\rangle$ in prior DLS analysis displayed notable increase with reduced system temperature. These combined trends, consistent with an early cumulant analysis, imply an increasingly more compact interior structure of colloidal aggregates that eventually drives the sol−gel transition. Thus, the bulk feature of MEH-PPV solution during the phase transition would appear to alter little (as can also be seen from Figure 10a), except for the gradual arresting of a certain fraction of colloidal aggregates. In contrast, polymer sol−gel transition is customarily associated with increasing number and size of aggregate clusters (with gradually reduced population of single chains) that later cross-link to form the gel network. The disparities both in the underlying structural feature and in the bridging mechanism might explain the lack of a power-law behavior in $|g^{(1)}(q,t)|$ (or $g^{(2)}(q,t) - 1$) as can often be observed with polymer gels.

3.3.4. Dynamic Modulus Measurement. To gain additional (mechanical) insight into MEH-PPV sol−gel transition, frequency sweep (at a strain magnitude of 0.3) was carried out from the solution state at 50 °C to the final gelation state (aging at 30 °C), and the results are shown in Figure 11. Upon decreasing the system temperature in solution state (Figure 11a), the magnitude of G' at low frequencies can be seen to increase dramatically. Meanwhile, the crossover of G' and G'' shifts systematically toward the high-frequency regime, indicative of an increasingly confined (i.e., more localized) "flow" region. These viscometric features, in fact, are quite similar to what had been observed for weakly attractive carbon black particles during sol−gel transition.[81]

It is of particular interest to note that, at a system temperature of 40 °C prior to gelation, the solid-like plateau of G' at low frequencies is very pronounced already, whereas all three DLS modes analyzed in Figure 5 showed no sign of deviating from the usual diffusive attributes. A rough estimate (i.e., $\tau_{DLS} \sim 2\pi/\omega$) suggests that, for the range of decay times (τ_{DLS} < 1s) of all three DLS modes, it would require a frequency greater than 5−10 rad/s to well observe the corresponding viscometric response. Thus, the solid-like behavior of G' for the solution sample as observed at frequencies substantially lower than the above estimate should be reflecting, instead, a condition when free diffusion becomes notably hindered at still longer elapsed times inaccessible by typical DLS analysis. The way these two protocols complement each other in general and in this study should be clear.

After 4-h aging at the gelation temperature 30 °C, Figure 11b shows that G' eventually grows to dominate over G'' and, given the arresting of the DLS slow mode at this stage, the plateau regime now effectively extends to a frequency as high as ∼10 rad/s. At still higher frequencies, it can be seen that G' continues to rise slightly, consistent with a prior observation that the DLS fast mode remained unbound even at a late stage of gelation. Another interesting feature in Figure 11b is that, with prolonged aging time, G' keeps growing substantially while G'' varies only marginally. As implied by the following kinetic analysis, this later stage of gelation coincides with an apparent (3-D) interweaving of previously fabricated (1-D) colloidal strands to further strengthen the elasticity of the bulk gel. Recall also that all light scattering features become relatively unchanged up to this point.

DOI: 10.1021/acs.jpcb.5b00575
J. Phys. Chem. B 2015, 119, 3320−3331

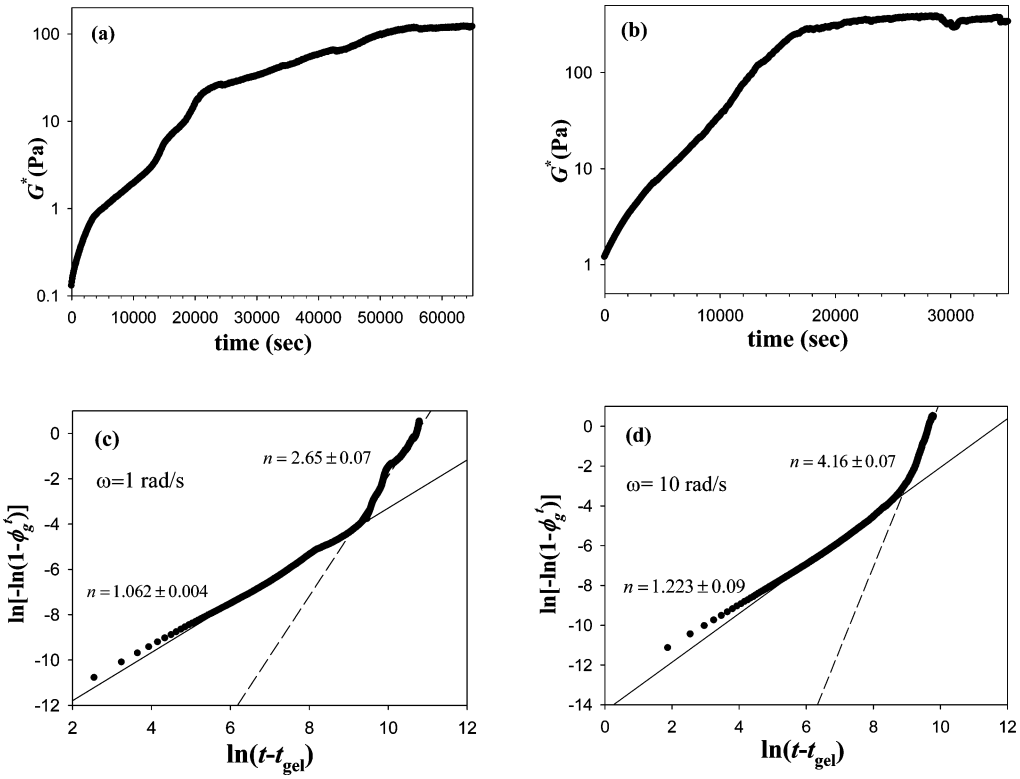

Figure 12. Complex modulus as a function of sweeping time at (a) ω = 1 rad/s and (b) ω = 10 rad/s. The corresponding data plotted in the linearized form (eq 6) are shown in (c) and (d), respectively.

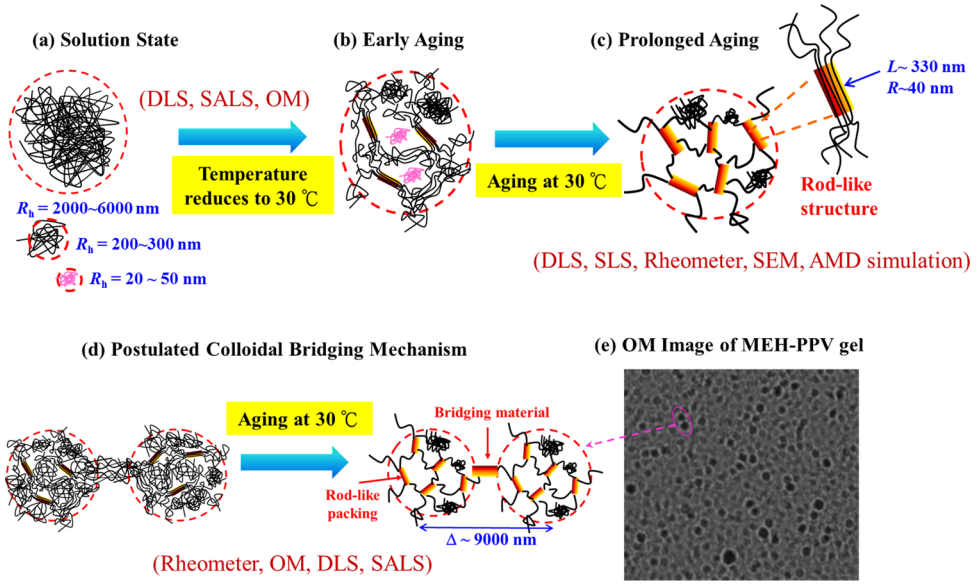

Figure 13. Schematic illustration of the structural evolution during MEH-PPV sol−gel transition; the OM image shown was taken from a freely evaporated gel sample to enhance the contrast.

Figure 12a-b shows the complex modulus G^* as a function of time at 30 °C for ω = 1 rad/s and ω = 10 rad/s, respectively. According to the discussion above, it can be expected that, whereas the complex modulus response at ω = 1 rad/s reflects the bulk feature of MEH-PPV gelation that is beyond the reach of typical DLS analysis, the response at ω = 10 rad/s should be, to some extent, reminiscent of the DLS slow- and intermediate-mode. A commonly utilized method to unveil the gelation kinetics is to analyze the variation of G^* with gelation time through the Avrami equation:[32,53]

$$\ln[-\ln(1-\phi_g^t)] = n[\ln k + \ln(t - t_{gel})] \quad (6)$$

where n is the Avrami component that reflects the fractal dimension of the gel structure, k is a rate constant proportional to the rate of gel growth, and t and t_{gel} are the elapsed time and the initial gelation time (i.e., at $G' = G''$), respectively. The extent of gelation (ϕ_g^t) can be expressed in terms of G^* at

DOI: 10.1021/acs.jpcb.5b00575
J. Phys. Chem. B 2015, 119, 3320−3331

different times as $\phi_g^t = ((G^*(t) - G^*_{bkg})/(G^*_{max} - G^*_{bkg}))$, where $G^*(t)$ is the time-dependent complex modulus, G^*_{bkg} is the complex modulus at the initial gelation time, and G^*_{max} is the maximum complex modulus at kinetic equilibrium. Here, G^*_{max} was taken from the mean value of the modulus data at long times when no appreciable changes were noticed.

Figure 12c,d shows the corresponding data that were plotted in the form of eq 6. In these plots, the slope yields the fractal dimension of the structure under development. A common feature for both frequencies is that the slope changes abruptly at some intermediate time (about 4-h aging) coincident with the time when a rapid growth of G' becomes evident in Figure 11b. The fractal dimensions were seen to alter from a value of about unity to somewhere around three. A relatively large deviation from this average trend can be noticed with the case of ω = 10 rad/s, where the result might as well be reflecting more localized dynamic events such as the structural reorganization *within* colloidal aggregates. Overall, the above features of time-sweep dynamic modulus clearly imply a 1-D to 3-D kinetic pathway of MEH-PPV gelation.

Prior work on the gels formed by a crystalline type of conjugated polymer (i.e., P3HT) had envisioned a similar 1-D to 3-D pathway of gelation.[32,36,37] We, however, have disclosed herein a somewhat different gelation mechanism for an amorphous conjugated polymer, which evidently capitalized on *colloidal-particle* bridging rather than direct interconnection of fibrous strands—which, for instance, may be readily built up for a crystalline conjugated polymer even in solution state.[15] What remains unclear is if similar fibrous materials as those developed within a colloidal aggregate might serve as the exterior bridging agent to fabricate interconnected colloidal strands. As is evident in Figure 7, the emergence of the q-independent intermediate mode occurred concomitantly with the arrested slow mode indicative of the onset of colloidal binding. Therefore, the above-suggested role of these fibrous materials seems plausible. In the absence of strong van der Waals interactions, as customarily associated with the binding of real colloidal particles, a possible mechanism of colloidal bridging is proposed in Figure 13 summarizing the overall findings and central implications from this study.

4. CONCLUSIONS

Figure 13 pictorially summarizes the structural evolution during MEH-PPV sol−gel transition in a hybrid-solvent medium; the exploratory schemes utilized at various stages are also shown for verification. MEH-PPV had been known to develop principally nanometer-sized aggregate species in commonly used solvents, and was occasionally observed to turn into gels under certain (harsh) experimental conditions without a clear clue to the underlying structures and mechanisms. Herein, MEH-PPV has been revealed, for the first time, to sustain an abundance of micrometer-sized colloidal aggregates in an ideally compromised hybrid-solvent medium without encountering first bulk phase separation, consequently rendering it possible to produce gel at relatively low concentration (<1 wt %) in a room-temperature aging process. The colloidal aggregates so fostered seemed featureless in solution and, upon gelation, morphed into "microgels" embodying a (porous) fibrous network as predicted by recent molecular dynamics simulation (see Figures S12−S14 in the SI). Although yet to be confirmed, the near coincidence of the above-mentioned microscopic and macroscopic phase alterations led us to contend that similar fibrous materials were involved in the bridging of colloidal aggregates to form colloidal strands, which can be clearly viewed from the OM image and further evidenced by time-sweep dynamic modulus response.

In the context of polymer gels, we noticed that the primary polymer gels known to utilize colloidal association are biological ones,[56,57] which ubiquitously involve smaller (nanometer-sized) aggregates and anisotropic interactions (such as hydrogen or hydrophobic bonds). Crystalline conjugated polymers, on the other hand, possess prominent $\pi-\pi$ interactions in solution and can thus readily foster interconnected fibrous materials and produce gels. These two close analogies, along with the curious lack of a power-law behavior in $|g^{(1)}(q,t)|$, help highlight the peculiarity of the MEH-PPV gel as has been explored herein. In a future perspective, the present findings shed light on the prospect of capitalizing on specific (hybrid) solvent media to incubate desirable colloidal aggregates and gels in room-temperature processing of practical valuable conjugated polymers.[82]

■ ASSOCIATED CONTENT

Supporting Information

Detailed information about the UV−vis absorption spectra of MEH-PPV solution and gel, the effect of incident light intensity on DLS feature, assessments of ergodicity for MEH-PPV gel, detailed descriptions of optical arrangement, calibration, and analyzing scheme of the SALS apparatus, DLS data on MEH-PPV/chlorobenzene solution, OM and SEM images of MEH-PPV gels, and molecular dynamics simulation results. This material is available free of charge via the Internet at http://pubs.acs.org.

■ AUTHOR INFORMATION

Corresponding Author

*E-mail: chmcch@ccu.edu.tw.

Notes

The authors declare no competing financial interest.

■ ACKNOWLEDGMENTS

This work is sponsored by the National Science Council of ROC. Resources provided by the National Center for High-Performance Computing of ROC are acknowledged.

■ REFERENCES

(1) Burroughes, J. H.; Bradley, D. D. C.; Brown, A. R.; Marks, R. N.; Mackay, K.; Friend, R. H.; Burns, P. L.; Holmes, A. B. Light-Emitting Diodes Based on Conjugated Polymers. *Nature* **1990**, *347*, 539−541.

(2) Braun, D.; Heeger, A. J. Visible Light Emission from Semiconducting Polymer Diodes. *Appl. Phys. Lett.* **1991**, *58*, 1982−1984.

(3) Friend, R. H.; Gymer, R. W.; Holmes, A. B.; Burroughes, J. H.; Marks, R. N.; Taliani, C.; Bradley, D. D. C.; Santos, D. A. D.; Brédas, J. L.; Lögdlund, M.; Salaneck, W. R. Electroluminescence in Conjugated Polymers. *Nature* **1999**, *397*, 121−128.

(4) Yu, G.; Gao, J.; Hummelen, J. C.; Wudl, F.; Heeger, A. J. Polymer Photovoltaic Cells: Enhanced Efficiencies via a Network of Internal Donor-Acceptor Heterojunctions. *Science* **1995**, *270*, 1789−1791.

(5) Halls, J. J. M.; Walsh, C. A.; Greenham, N. C.; Marseglia, E. A.; Friend, R. H.; Moratti, S. C.; Holmes, A. B. Efficient Photodiodes from Interpenetrating Polymer Networks. *Nature* **1995**, *376*, 498−500.

(6) Dennler, G.; Scharber, M. C.; Brabec, C. J. Polymer−Fullerene Bulk-Heterojunction Solar Cells. *Adv. Mater.* **2009**, *21*, 1323−1338.

(7) Nguyen, T.-Q.; Doan, V.; Schwartz, B. J. Conjugated Polymer Aggregates in Solution: Control of Interchain Interactions. *J. Chem. Phys.* **1999**, *110*, 4068−4078.

DOI: 10.1021/acs.jpcb.5b00575
J. Phys. Chem. B 2015, 119, 3320−3331

(8) Banach, M. J.; Friend, R. H.; Sirringhaus, H. Influence of the Casting Solvent on the Thermotropic Alignment of Thin Liquid Crystalline Polyfluorene Copolymer Films. *Macromolecules* **2004**, *37*, 6079−6085.
(9) Mahfoud, A.; Sarangan, A.; Nelson, T. R.; Blubaugh, E. A. Role of Aggregation in the Amplified Spontaneous Emission of [2-methoxy-5-(2′-ethylhexyloxy)-1,4-phenylenevinylene] in Solution and Films. *J. Lumin.* **2006**, *118*, 123−130.
(10) Collison, C. J.; Rothberg, L. J.; Treemaneekarn, V.; Li, Y. Conformational Effects on the Photophysics of Conjugated Polymers: A Two Species Model for MEH−PPV Spectroscopy and Dynamics. *Macromolecules* **2001**, *34*, 2346−2352.
(11) Quan, S.; Teng, F.; Xu, Z.; Qian, L.; Hou, Y.; Wang, Y.; Xu, X. Solvent and Concentration Effects on Fluorescence Emission in MEH-PPV Solution. *Eur. Polym. J.* **2006**, *42*, 228−233.
(12) Ou-Yang, W.-C.; Chang, C.-S.; Chen, H.-L.; Tsao, C.-S.; Peng, K.-Y.; Chen, S.-A.; Han, C. Micellelike Aggregates in Solutions of Semirigid Hairy-Rod Polymers. *Phys. Rev. E* **2005**, *72*, 031802.
(13) Li, Y. C.; Chen, C. Y.; Chang, Y. X.; Chuang, P. Y.; Chen, J. H.; Chen, H. L.; Hsu, C. S.; Ivanov, V. A.; Khalatur, P. G.; Chen, S. A. Scattering Study of the Conformational Structure and Aggregation Behavior of a Conjugated Polymer Solution. *Langmuir* **2009**, *25*, 4668−4677.
(14) Knaapila, M.; Garamus, V. M.; Dias, F. B.; Almásy, L.; Galbrecht, F.; Charas, A.; Morgado, J.; Burrows, H. D.; Scherf, U.; Monkman, A. P. Influence of Solvent Quality on the Self-Organization of Archetypical Hairy Rods−Branched and Linear Side Chain Polyfluorenes: Rodlike Chains versus "Beta-Sheets" in Solution. *Macromolecules* **2006**, *39*, 6505−6512.
(15) Newbloom, G. M.; Kim, F. S.; Jenekhe, S. A.; Pozzo, D. C. Mesoscale Morphology and Charge Transport in Colloidal Networks of Poly(3-hexylthiophene). *Macromolecules* **2011**, *44*, 3801−3809.
(16) Hua, C. C.; Lin, C. J.; Wen, Y. H.; Chen, S. A. Stabilization of Bulk Aggregation State in Semiconducting Polymer Solutions. *J. Polym. Res.* **2011**, *18*, 793−800.
(17) Wen, Y. H.; Lin, P. C.; Hua, C. C.; Chen, S. A. Dynamic Structure Factor for Large Aggregate Clusters with Internal Motions: A Self-Consistent Light-Scattering Study on Conjugated Polymer Solutions. *J. Phys. Chem. B* **2011**, *115*, 14369−14380.
(18) Petekidis, G.; Vlassopoulos, D.; Fytas, G.; Fleischer, G. Dynamics of Hairy-Rod Polymers: Semidilute Regime. *Macromolecules* **1998**, *31*, 1406−1417.
(19) Lee, C. K.; Hua, C. C.; Chen, S. A. Single-Chain and Aggregation Properties of Semiconducting Polymer Solutions Investigated by Coarse-Grained Langevin Dynamics Simulation. *J. Phys. Chem. B* **2008**, *112*, 11479−11489.
(20) Lee, C. K.; Hua, C. C.; Chen, S. A. Multiscale Simulation for Conducting Conjugated Polymers from Solution to the Quenching State. *J. Phys. Chem. B* **2009**, *113*, 15937−15948.
(21) Lee, C. K.; Hua, C. C.; Chen, S. A. Hybrid Solvents Incubated $\pi-\pi$ Stacking in Quenched Conjugated Polymer Resolved by Multiscale Computation. *Macromolecules* **2011**, *44*, 320−324.
(22) Fizazi, A.; Moulton, J.; Pakbaz, K.; Rughooputh, S. D. D. V.; Smith, P.; Heeger, A. J. Percolation on a Self-Assembled Network: Decoration of Polyethylene Gels with Conducting Polymer. *Phys. Rev. Lett.* **1990**, *64*, 2180−2183.
(23) Pépin-Donat, B.; Viallat, A.; Blachot, J. F.; Lombard, C. Electromechanical Polymer Gels Combining Rubber Elasticity with Electronic Conduction. *Adv. Mater.* **2006**, *18*, 1401−1405.
(24) Tiitu, M.; Hiekkataipale, P.; Hartikainen, J.; Mäkelä, T.; Ikkala, O. Viscoelastic and Electrical Transitions in Gelation of Electrically Conducting Polyaniline. *Macromolecules* **2002**, *35*, 5212−5217.
(25) Chang, S. C.; Yang, Y. Polymer Gel Light-Emitting Devices. *Appl. Phys. Lett.* **1999**, *75*, 2713−2715.
(26) Kim, B. G.; Jeong, E. J.; Park, H. J.; Bilby, D.; Guo, L. J.; Kim, J. Effect of Polymer Aggregation on the Open Circuit Voltage in Organic Photovoltaic Cells: Aggregation-Induced Conjugated Polymer Gel and Its Application for Preventing Open Circuit Voltage Drop. *ACS Appl. Mater. Interfaces* **2011**, *3*, 674−680.
(27) Huang, W. Y.; Huang, P. T.; Han, Y. K.; Lee, C. C.; Hsieh, T. L.; Chang, M. Y. Aggregation and Gelation Effects on the Performance of Poly(3-hexylthiophene)/Fullerene Solar Cells. *Macromolecules* **2008**, *41*, 7485−7489.
(28) Chang, M.-Y.; Huang, Y.-H.; Han, Y.-K. Aggregation, Crystallization, and Resistance Properties of Poly(3-hexylthiophene-2,5-diyl) Solid Films Gel-Cast from $CHCl_3$/p-Xylene Mixed Solvents. *Org. Electron* **2014**, *15*, 251−259.
(29) Babu, S. S.; Praveen, V. K.; Ajayaghosh, A. Functional π-Gelators and Their Applications. *Chem. Rev.* **2014**, *114*, 1973−2129.
(30) Yang, C. Y.; Heeger, A. J.; Cao, Y. Microstructure of Gel-Processed Blends of Conjugated Polymer and Ultrahigh Molecular Weight Polyethylene. *Polymer* **2000**, *41*, 4113−4118.
(31) Alcazar, D.; Wang, F.; Swager, T. M.; Thomas, E. L. Gel Processing for Highly Oriented Conjugated Polymer Films. *Macromolecules* **2008**, *41*, 9863−9868.
(32) Newbloom, G. M.; Weigandt, K. M.; Pozzo, D. C. Electrical, Mechanical, and Structural Characterization of Self-Assembly in Poly(3-hexylthiophene) Organogel Networks. *Macromolecules* **2012**, *45*, 3452−3462.
(33) Viallat, A.; Pépin-Donat, B. State of Gelation of Fully Conjugated Conducting Gels. Gel Fraction, Swelling, and Nuclear Magnetic Relaxation. *Macromolecules* **1997**, *30*, 4679−4687.
(34) Malik, S.; Jana, T.; Nandi, A. K. Thermoreversible Gelation of Regioregular Poly(3-hexylthiophene) in Xylene. *Macromolecules* **2001**, *34*, 275−282.
(35) Chen, C.-Y.; Chan, S.-H.; Li, J.-Y.; Wu, K.-H.; Chen, H.-L.; Chen, J.-H.; Huang, W.-Y.; Chen, S.-A. Formation and Thermally-Induced Disruption of Nanowhiskers in Poly(3-hexylthiophene)/Xylene Gel Studied by Small-Angle X-ray Scattering. *Macromolecules* **2010**, *43*, 7305−7311.
(36) Koppe, M.; Brabec, C. J.; Heiml, S.; Schausberger, A.; Duffy, W.; Heeney, M.; McCulloch, I. Influence of Molecular Weight Distribution on the Gelation of P3HT and Its Impact on the Photovoltaic Performance. *Macromolecules* **2009**, *42*, 4661−4666.
(37) Xu, W.; Tang, H.; Lv, H.; Li, J.; Zhao, X.; Li, H.; Wang, N.; Yang, X. Sol-Gel Transition of Poly(3-hexylthiophene) Revealed by Capillary Measurements: Phase Behaviors, Gelation Kinetics and the Formation Mechanism. *Soft Matter* **2012**, *8*, 726−733.
(38) Huang, W. Y.; Matsuoka, S.; Kwei, T. K.; Okamoto, Y. Aggregation and Gelation of Fully Conjugated Rigid-Rod Polymers. Poly(2,5-dialkyl-1,4-phenyleneethynylene)s. *Macromolecules* **2001**, *34*, 7166−7171.
(39) Perahia, D.; Traiphol, R.; Bunz, U. H. F. From Single Molecules to Aggregates to Gels in Dilute Solution: Self-Organization of Nanoscale Rodlike Molecules. *J. Chem. Phys.* **2002**, *117*, 1827−1832.
(40) Chen, C.-Y.; Chang, C.-S.; Huang, S.-W.; Chen, J.-H.; Chen, H.-L.; Su, C.-I.; Chen, S.-A. Phase-Separation-Induced Gelation of Poly(9,9-dioctylfluorene)/Methylcyclohexane Solution. *Macromolecules* **2010**, *43*, 4346−4354.
(41) Lin, Z.-Q.; Shi, N.-E.; Li, Y.-B.; Qiu, D.; Zhang, L.; Lin, J.-Y.; Zhao, J.-F.; Wang, C.; Xie, L.-H.; Huang, W. Preparation and Characterization of Polyfluorene-Based Supramolecular π-Conjugated Polymer Gels. *J. Phys. Chem. C* **2011**, *115*, 4418−4424.
(42) Chen, S. H.; Su, A. C.; Chang, C. S.; Chen, H. L.; Ho, D. L.; Tsao, C. S.; Peng, K. Y.; Chen, S. A. Aging of Poly(2-methoxy-5-(2′-ethylhexyloxy)-1,4-phenylenevinylene)/Toluene Solutions and Subsequent Effects on Luminescence Behavior of Cast Films. *Langmuir* **2004**, *20*, 8909−8915.
(43) Hua, C. C.; Chen, C. L.; Chang, C. W.; Lee, C. K.; Chen, S. A. Viscometric Investigation of Aggregate Formation in Dilute Conjugated Polymer Solutions. *J. Rheol.* **2005**, *49*, 641−656.
(44) Wang, P.-S.; Lu, H.-H.; Liu, C.-Y.; Chen, S.-A. Gel Formation via Physical Cross-Linking in the Soluble Conjugated Polymer, Poly[2-methoxy-5-(2-ethylhexyloxy)-1,4-phenylenevinylene], in Solution by Addition of Alkanes. *Macromolecules* **2008**, *41*, 6500−6504.
(45) Chen, J.-H.; Chiu, C.-W.; Chen, L.-C.; Lai, S.-Y.; Lee, C.-C. Conformational Structure and Aggregation Behavior of Poly[2-

DOI: 10.1021/acs.jpcb.5b00575
J. Phys. Chem. B 2015, 119, 3320−3331

methoxy-5-(2-ethylhexyloxy)-1,4-phenylenevinylene] in Toluene/Nonane Solutions. *Polymer* **2012**, *53*, 4843−4854.
(46) Mallia, V. A.; Butler, P. D.; Sarkar, B.; Holman, K. T.; Weiss, R. G. Reversible Phase Transitions within Self-Assembled Fibrillar Networks of (*R*)-18-(*n*-Alkylamino)octadecan-7-ols in Their Carbon Tetrachloride Gels. *J. Am. Chem. Soc.* **2011**, *133*, 15045−15054.
(47) Mallia, V. A.; Terech, P.; Weiss, R. G. Correlations of Properties and Structures at Different Length Scales of Hydro- and Organo-gels Based on *N*-Alkyl-(*R*)-12-Hydroxyoctadecylammonium Chlorides. *J. Phys. Chem. B* **2011**, *115*, 12401−12414.
(48) Toro-Vazquez, J. F.; Morales-Rueda, J.; Torres-Martinez, A.; Charo-Alonso, M. A.; Mallia, V. A.; Weiss, R. G. Cooling Rate Effects on the Microstructure, Solid Content, and Rheological Properties of Organogels of Amides Derived from Stearic and (*R*)-12-Hydroxystearic Acid in Vegetable Oil. *Langmuir* **2013**, *29*, 7642−7654.
(49) Terech, P.; Weiss, R. G. Low Molecular Mass Gelators of Organic Liquids and the Properties of Their Gels. *Chem. Rev.* **1997**, *97*, 3133−3160.
(50) Ngai, T.; Wu, C.; Chen, Y. Origins of the Speckles and Slow Dynamics of Polymer Gels. *J. Phys. Chem. B* **2004**, *108*, 5532−5540.
(51) Shibayama, M.; Tsujimoto, M.; Ikkai, F. Static Inhomogeneities in Physical Gels: Comparison of Temperature-Induced and Concentration-Induced Sol−Gel Transition. *Macromolecules* **2000**, *33*, 7868−7876.
(52) Kjøniksen, A.-L.; Nyström, B. Dynamic Light Scattering of Poly(vinyl alcohol) Solutions and Their Dynamical Behavior during the Chemical Gelation Process. *Macromolecules* **1996**, *29*, 7116−7123.
(53) Huang, X.; Raghavan, S. R.; Terech, P.; Weiss, R. G. Distinct Kinetic Pathways Generate Organogel Networks with Contrasting Fractality and Thixotropic Properties. *J. Am. Chem. Soc.* **2006**, *128*, 15341−15352.
(54) Lee, C. K.; Hua, C. C.; Chen, S. A. Phase Transition and Gels in Conjugated Polymer Solutions. *Macromolecules* **2013**, *46*, 1932−1938.
(55) Tanaka, F. *Polymer Physics: Applications to Molecular Association and Thermoreversible Gelation*; Cambridge University Press: New York, 2011.
(56) Ikeda, S.; Foegeding, E. A.; Hagiwara, T. Rheological Study on the Fractal Nature of the Protein Gel Structure. *Langmuir* **1999**, *15*, 8584−8589.
(57) Kontogiorgos, V.; Vaikousi, H.; Lazaridou, A.; Biliaderis, C. G. A Fractal Analysis Approach to Viscoelasticity of Physically Cross-Linked Barley *β*-Glucan Gel Networks. *Colloids Surf., B* **2006**, *49*, 145−152.
(58) Parashchuk, O. D.; Laptinskaya, T. V.; Ananieva, M. S.; Paraschuk, D. Y. Hyperdiffusive Dynamics in Conjugated Polymer Blends and Fullerene Absorbing Solutions. *Soft Matter* **2011**, *7*, 5585−5594.
(59) Siegert, A. J. F. *MIT Radiation Lab. Report*, 1943, No. 475.
(60) Berne, B. J.; Pecora, R. *Dynamic Light Scattering: With Applications to Chemistry, Biology, and Physics*; Dover: New York, 2000.
(61) Provenchers, S. W. A Constrained Regularization Method for Inverting Data Represented by Linear Algebraic or Integral Equations. *Comput. Phys. Commun.* **1982**, *27*, 213−227.
(62) Klucker, R.; Munch, J. P.; Schosseler, F. Combined Static and Dynamic Light Scattering Study of Associating Random Block Copolymers in Solution. *Macromolecules* **1997**, *30*, 3839−3848.
(63) Buhler, E.; Rinaudo, M. Structural and Dynamical Properties of Semirigid Polyelectrolyte Solutions: A Light-Scattering Study. *Macromolecules* **2000**, *33*, 2098−2106.
(64) Hermans, T. M.; Broeren, M. A. C.; Gomopoulos, N.; van der Schoot, P.; van Genderen, M. H. P.; Sommerdijk, N. A. J. M.; Fytas, G.; Meijer, E. W. Self-Assembly of Soft Nanoparticles with Tunable Patchiness. *Nat. Nanotechnol.* **2009**, *4*, 721−726.
(65) Ferri, F. Use of A Charge Coupled Device Camera for Low-Angle Elastic Light Scattering. *Rev. Sci. Instrum.* **1997**, *68*, 2265−2274.
(66) Martin, J. E.; Wilcoxon, J.; Odinek, J. Decay of Density Fluctuations in Gels. *Phys. Rev. A* **1991**, *43*, 858−872.
(67) Norisuye, T.; Takeda, M.; Shibayama, M. Cluster-Size Distribution of Cross-Linked Polymer Chains across the Gelation Threshold. *Macromolecules* **1998**, *31*, 5316−5322.
(68) Norisuye, T.; Shibayama, M.; Tamaki, R.; Chujo, Y. Time-Resolved Dynamic Light Scattering Studies on Gelation Process of Organic−Inorganic Polymer Hybrids. *Macromolecules* **1999**, *32*, 1528−1533.
(69) Okamoto, M.; Norisuye, T.; Shibayama, M. Time-Resolved Dynamic Light Scattering Study on Gelation and Gel-Melting Processes of Gelatin Gels. *Macromolecules* **2001**, *34*, 8496−8502.
(70) Aoki, Y.; Norisuye, T.; Tran-Cong-Miyata, Q.; Nomura, S.; Sugimoto, T. Dynamic Light Scattering Studies on Network Formation of Bridged Polysilsesquioxanes Catalyzed by Polyoxometalates. *Macromolecules* **2003**, *36*, 9935−9942.
(71) Wu, C.; Chan, K. K.; Xia, K.-Q. Experimental Study of the Spectral Distribution of the Light Scattered from Flexible Macromolecules in Very Dilute Solution. *Macromolecules* **1995**, *28*, 1032−1037.
(72) Doi, M.; Edwards, S. F. *The Theory of Polymer Dynamics*; Oxford Univeristy Press: New York, 1986.
(73) Koike, A.; Nemoto, N.; Inoue, T.; Osaki, K. Dynamic Light Scattering and Dynamic Viscoelasticity of Poly(vinyl alcohol) in Aqueous Borax Solutions. 1. Concentration Effect. *Macromolecules* **1995**, *28*, 2339−2344.
(74) Johannsson, R.; Chassenieux, C.; Durand, D.; Nicolai, T.; Vanhoorne, P.; Jerome, R. Dynamic Properties of the Transient Network Formed by Telechelic Ionomers Studied by Dynamic Light Scattering and Dynamic Mechanical Analysis. *Macromolecules* **1995**, *28*, 8504−8510.
(75) Thuresson, K.; Nilsson, S.; Kjøniksen, A.-L.; Walderhaug, H.; Lindman, B.; Nyström, B. Dynamics and Rheology in Aqueous Solutions of Associating Diblock and Triblock Copolymers of the Same Type. *J. Phys. Chem. B* **1999**, *103*, 1425−1436.
(76) Fytas, G.; Nothofer, H. G.; Scherf, U.; Vlassopoulos, D.; Meier, G. Structure and Dynamics of Nondilute Polyfluorene Solutions. *Macromolecules* **2002**, *35*, 481−488.
(77) Li, J.; Li, W.; Huo, H.; Luo, S.; Wu, C. Reexamination of the Slow Mode in Semidilute Polymer Solutions: The Effect of Solvent Quality. *Macromolecules* **2008**, *41*, 901−911.
(78) Asnaghi, D.; Giglio, M.; Bossi, A.; Righetti, P. G. Quasi-Ordered Structure in Highly Cross-Linked Poly(acrylamide) Gels. *Macromolecules* **1997**, *30*, 6194−6198.
(79) Hirokawa, Y.; Okamoto, T.; Kimishima, K.; Jinnai, H.; Koizumi, S.; Aizawa, K.; Hashimoto, T. Sponge-like Heterogeneous Gels: Hierarchical Structures in Poly(*N*-isopropylacrylamide) Chemical Gels As Observed by Combined Scattering and Confocal Microscopy Method. *Macromolecules* **2008**, *41*, 8210−8219.
(80) Shibayama, M.; Tanaka, T.; Han, C. C. Small Angle Neutron Scattering Study on Poly(*N*-isopropyl acrylamide) Gels Near Their Volume-Phase Transition Temperature. *J. Chem. Phys.* **1992**, *97*, 6829−6841.
(81) Trappe, V.; Weitz, D. A. Scaling of the Viscoelasticity of Weakly Attractive Particles. *Phys. Rev. Lett.* **2000**, *85*, 449−452.
(82) Newbloom, G. M.; de la Iglesia, P.; Pozzo, L. D. Controlled Gelation of Poly(3-alkylthiophene)s in Bulk and in Thin-Films Using Low Volatility Solvent/Poor-Solvent Mixtures. *Soft Matter* **2014**, *10*, 8945−8954.

DOI: 10.1021/acs.jpcb.5b00575
J. Phys. Chem. B 2015, 119, 3320−3331